Arabian Journal of Chemistry (2023) **16**, 105146

King Saud University

Arabian Journal of Chemistry

www.ksu.edu.sa
www.sciencedirect.com

ORIGINAL ARTICLE

Design, synthesis, and biological evaluation of 4-aryl-9*H*-carbazoles as tubulin polymerization inhibitors with potent anticancer activities

Chao Wang [a,b], Yujing Zhang [c,*], Shanbo Yang [a,b], Yutao Xiu [a,b], Wujun Chen [a,b], Yanhong Wang [a,b,*], Dongming Xing [a,b,d,*]

[a] *Cancer Institute, The Affiliated Hospital of Qingdao University, Qingdao University, Qingdao 266000, Shandong, China*
[b] *Qingdao Cancer Institute, Qingdao University, Qingdao 266000, Shandong, China*
[c] *The Affiliated Cardiovascular Hospital of Qingdao University, Qingdao University, Qingdao 266071, Shandong, China*
[d] *School of Life Sciences, Tsinghua University, Beijing 100084, China*

Received 8 May 2023; accepted 6 July 2023
Available online 11 July 2023

KEYWORDS

Carbazole;
Antiproliferative activity;
G2/M phase;
Tubulin polymerization inhibitors;
Molecular docking

Abstract Some novel 4-aryl-9*H*-carbazoles were designed as potential tubulin polymerization inhibitors through structural optimization and bioisosteric strategy. These compounds showed effective antiproliferative activities against a diverse set of cancer cell lines, including HeLa, HepG2, and SGC-7901 cells. Among them, compound **13k** exerted the strongest inhibitory effect on HeLa cells with an IC_{50} of 1.2 ± 0.09 μM. Mechanism studies indicated that **13k** significantly inhibited tubulin polymerization *in vitro* and disrupted the dynamic homeostasis of microtubules in HeLa cells. Furthermore, **13k** concentration-dependently caused G2/M phase cell cycle arrest and apoptosis in HeLa cells. Molecular docking analysis demonstrated the interaction of **13k** at the colchicine binding site of tubulin. In addition, the prediction of physicochemical properties studies shows that **13k** has good pharmacokinetic properties. These preliminary results suggested that **13k** is a new tubulin polymerization inhibitor and worthy of further investigation.

* Corresponding authors at: The Affiliated Cardiovascular Hospital of Qingdao University, Qingdao University, Qingdao 266071, Shandong, China (Yujing Zhang); Cancer Institute, The Affiliated Hospital of Qingdao University, Qingdao University, Qingdao 266000, Shandong, China (Yanhong Wang).
E-mail addresses: 459233223@qq.com (Y. Zhang), wangyh@qdu.edu.cn (Y. Wang), xdm_tsinghua@163.com (D. Xing).
Peer review under responsibility of King Saud University.

Production and hosting by Elsevier

1. Introduction

Microtubules are important structural elements in eukaryotic cells and are crucial for a number of fundamental cell processes, such as cell division, intracellular transport, and shape maintenance (Dumontet and Jordan, 2010; Steinmetz and Prota, 2018; Jordan and Wilson, 2004). The various roles that microtubules play during cell mitosis have made them a very desirable target for the development of novel anticancer drugs (Kaul et al., 2019; Lawrence and Zanic, 2019). It is commonly believed that microtubule-targeted drugs (MTAs) exhibit their anticancer activity *via* interaction with one of the six binding sites

https://doi.org/10.1016/j.arabjc.2023.105146
1878-5352

in microtubule proteins (colchicine site, laurimide site, mevalonate site, paclitaxel site, pyrantel site, and ventolin site), thereby impeding cancer cell proliferation, disrupting the dynamic equilibrium of microtubules, and resulting in cell death. MTAs for clinical use are those target the vinca or paclitaxel sites, e.g., vinca alkaloids and taxanes. MTAs have been used with great success in the treatment of various cancers such as breast, lung, ovarian, and prostate cancers (Cermak et al., 2020; Banerjee et al., 2018; Karahalil et al., 2019). Although clinical applications of MTAs binding to vinca or paclitaxel sites in tubulin have been extremely successful, there are no colchicine binding site anticancer drugs for clinical use (Wang et al., 2022; Arnst et al., 2019).

Colchicine binding site inhibitors (CBSIs) such as colchicine (**1**, Fig. 1), CA-4 (**2**, Fig. 1), *iso*CA-4 (**3**, Fig. 1), SMART (**4**, Fig. 1), MCP-6827 (**5**, Fig. 1), acridane (**6**, Fig. 1), XRP44X (**7**, Fig. 1), and ABT-751 (**8**, Fig. 1) are attractive to many research groups due to their potent potency and relatively simple chemical structure optimization (Egharevba et al., 2022; Zhang et al., 2023; Lu et al., 2009; Risinger et al., 2011; Wasylyk et al., 2008). Although those CBSIs can dramatically inhibit tubulin polymerization, these are limited in their therapeutic applications due to their poor water solubility, chemical instability, low bioavailability, or the emergence of multidrug resistance (Wang et al., 2019; Huang et al., 2020; Sherbet, 2020). In order to overcome the drawbacks of these CBSIs, there is a desire to find new MTAs that deliver their biological effects either through inhibition of tubulin assembly and suppression of microtubule formation.

Recently, the novel CBSI NSC676693 (**9**, Fig. 1) reported by Sylvain Rault *et al.* (Lisowski et al., 2004) displayed promising effects in inhibiting tubulin polymerization and the formation of actin cytoskeleton. It exhibited strong anticancer activity against human cancer cells with an IC_{50} in the nanomolar range. NSC676693 has been considered as a potential lead compound for tubulin polymerization inhibitors. The chemical structure of NSC676693 is composed of an aryl ring (A-ring) and a thienyl pyrrolidone molecular fragment (B-ring). Generally, the most favorite design strategy for NSC676693 analogs is to replace the B-ring with other heterocycles, depending on the bioisosteric strategy (Lisowski et al., 2004). This unique pharmacological feature, that is, the inhibition of tubulin polymerization, inspired us to proceed with the structural modification of NSC676693, leading to the potential development of more active anticancer drugs.

Carbazole-fused heterocycles have recently attracted growing interest as a specific backbone for the discovery of anticancer drugs. Intriguingly, its derivatives, such as IG-105 (**10**, Fig. 1) and compounds **11** and **12** (Fig. 1), exhibited excellent anticancer potencies and antitubulin activities at lower concentrations (Hu et al., 2007; Bzeih et al., 2016; Naret et al., 2019). Based on the above results, the stable fragment carbazole was selected to replace the B-ring of NSC676693 under the guidance of the bioisosteric strategy.

Herein, a set of 4-aryl-9*H*-carbazoles (**13**, Fig. 2) were designed and synthesized as new tubulin polymerization inhibitors. To explore the structure activity relationship of 4-aryl-9*H*-carbazoles, a variety of rigid heterocyclic rings were introduced in the A-ring. Preliminary *in vitro* bioactivity tests including antiproliferative activity, tubulin polymerization, immunofluorescence staining, cell cycle analysis, and apoptosis assay were conducted to exploration preliminary structure activity relationship and elucidation of pharmacological mechanisms. In addition, molecular docking analysis was performed to investigate the possible binding modes of the target compounds.

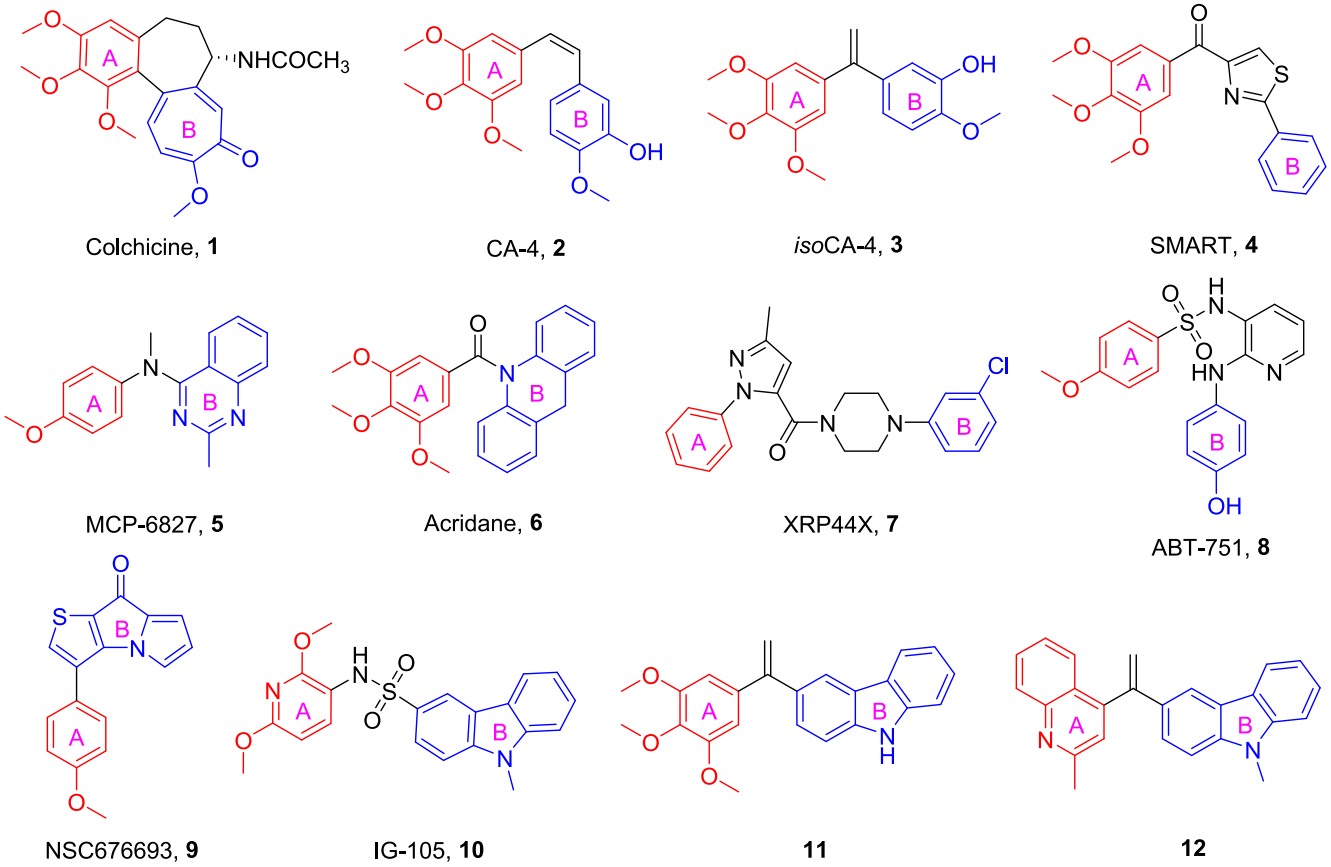

Fig. 1 Chemical structures of some representative CBSIs.

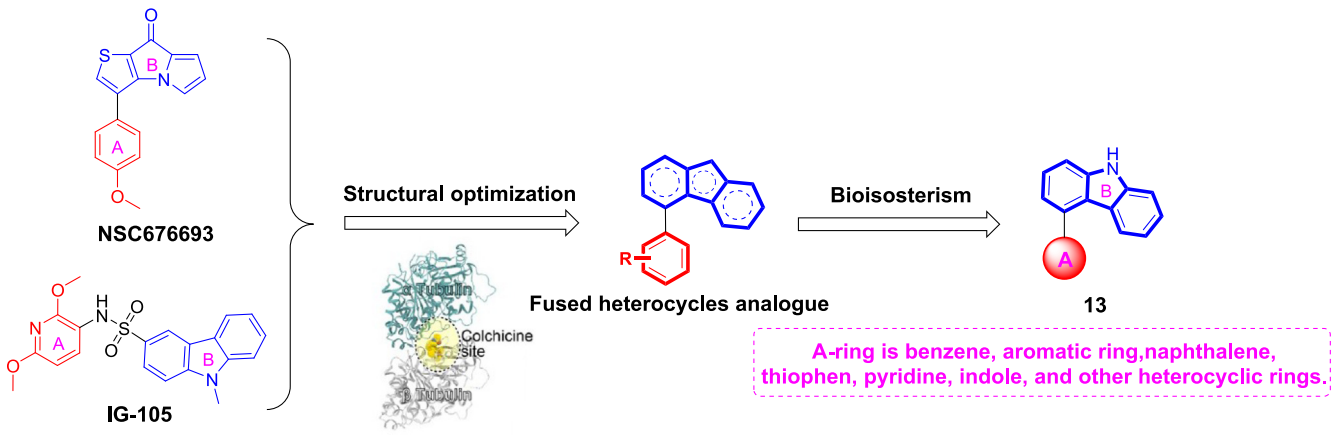

Fig. 2 The rational design of target compounds.

2. Result and discussion

2.1. Chemistry

Scheme 1 illustrates the general synthetic method for the preparation of 4-aryl-9*H*-carbazoles (**13**). First, commercially available (2-bromophenyl)boronic acid (**14**) was used as the starting material and reacted with 1-bromo-2-nitrobenzene (**15**) to produce 2-bromo-2′-nitro-1,1′-biphenyl (**16**) (Elmabruk et al., 2019). Subsequently, compound **16** was further reacted with PPh_3 in the presence of 1,2-dichlorobenzene to give key intermediate 4-bromo-9*H*-carbazole (**17**) at 120 °C (Ameen et al., 2018). Finally, the target compounds 4-aryl-9*H*-carbazoles (**13**) were generated *via* the Suzuki cross-coupling reaction between **17** and the corresponding arylboronic acid (Shi et al., 2022; Yang et al., 2022).

2.2. Biological evaluation

2.2.1. In vitro antiproliferative activity

The antiproliferative activities of the newly synthesized compounds **13a-u** were evaluated against three cancer cell lines (HeLa, HepG2, and SGC-7901) using a conventional MTT assay with CA-4 as the positive control. Most of the compounds exhibited moderate antiproliferative activities against the three tested cell lines with IC_{50} values in the micromolar range. These results indicated that the introduction of the carbazole moiety as a suitable mimic for the ternary heterocyclic

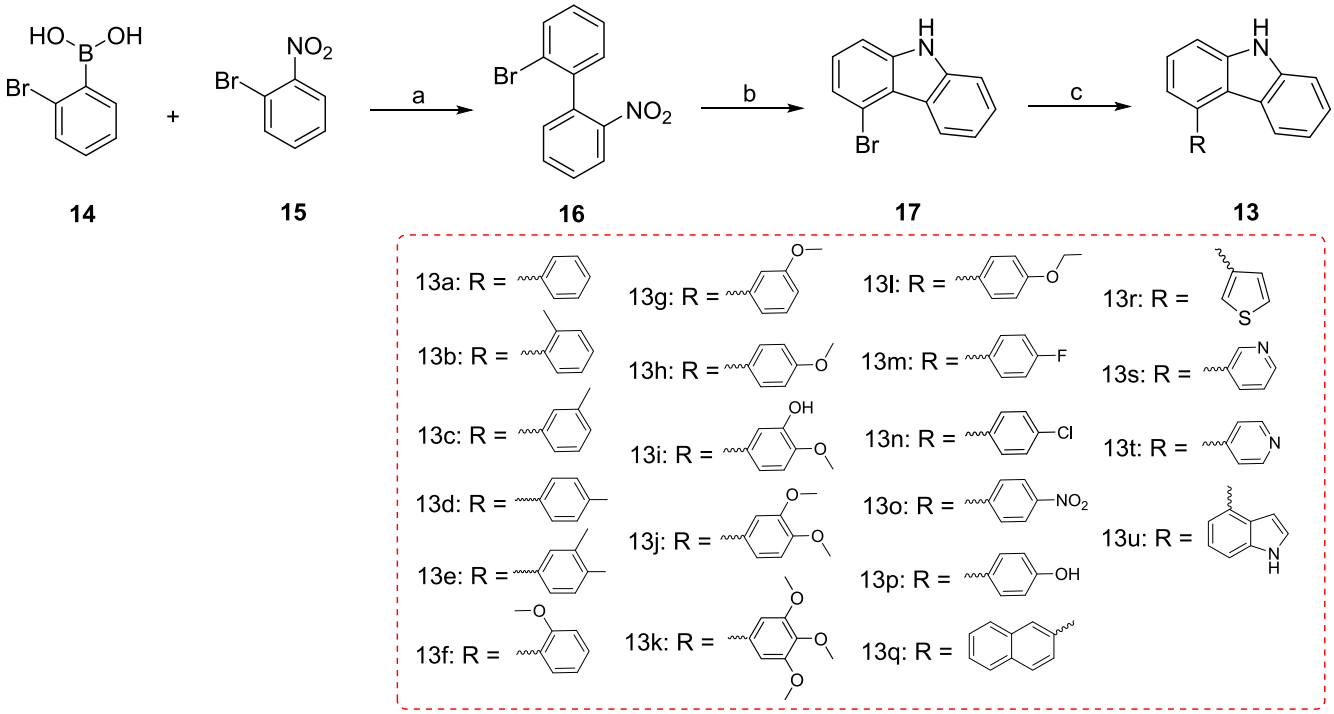

Scheme 1 Reagents and conditions (a) $Pd(PPh_3)_4$, K_2CO_3, THF/H_2O, N_2 atmosphere, 116 °C, M.W.; (b) PPh_3, 1,2-dichlorobenzene, 170 °C; (c) Substituted phenylboronic acid, $Pd(PPh_3)_4$, K_2CO_3, 1,4-dioxane/H_2O, N_2 atmosphere,126 °C, M.W..

Table 1 Antiproliferative activity of all compounds.

Compounds	(IC_{50} ± SD, μM)[a]		
	HeLa	HepG2	SGC-7901
13a	10.3 ± 1.3	12.4 ± 1.4	12.1 ± 1.5
13b	13.6 ± 1.2	16.3 ± 1.3	12.7 ± 1.0
13c	9.2 ± 0.90	11.6 ± 1.6	10.9 ± 1.4
13d	7.2 ± 0.81	10.0 ± 0.91	8.5 ± 0.62
13e	17.9 ± 1.8	> 30	20.1 ± 1.9
13f	8.2 ± 0.63	13.7 ± 1.8	11.9 ± 0.96
13 g	6.8 ± 0.42	9.7 ± 0.73	9.9 ± 1.1
13 h	3.4 ± 0.23	5.5 ± 0.34	4.0 ± 0.35
13i	> 30	20.5 ± 2.1	> 30
13j	11.5 ± 0.7	> 30	9.5 ± 1.0
13k	**1.2 ± 0.09**	**2.2 ± 0.17**	**2.0 ± 0.10**
13l	6.4 ± 0.53	7.5 ± 0.47	8.0 ± 0.75
13m	19.6 ± 1.4	23.3 ± 2.3	22.8 ± 1.9
13n	21.8 ± 2.1	25.8 ± 2.6	> 30
13o	> 30	29.1 ± 3.1	> 30
13p	10.6 ± 0.77	11.9 ± 1.2	9.2 ± 0.63
13q	20.6 ± 1.7	17.3 ± 2.3	16.7 ± 1.6
13r	25.5 ± 1.9	> 30	27.9 ± 2.6
13s	> 30	> 30	> 30
13t	28.9 ± 3.0	> 30	22.9 ± 2.1
13u	10.8 ± 0.99	12.6 ± 1.5	13.1 ± 1.7
CA-4[b]	0.089 ± 0.006	0.12 ± 0.01	0.097 ± 0.008

[a] IC_{50}: the half maximal inhibitory concentration.
[b] Used as positive controls.

ring present in NSC676693 maintained the effective antiproliferative activity.

We first introduced different rigid aromatic groups such as phenyl (**13a**), naphthyl (**13q**), thienyl (**13r**), pyridyl (**13s** and **13t**), and indolyl (**13u**) into the A-ring to explore the effect of different skeletons on antiproliferative activities against three different cell lines. As shown in Table 1, benzene derivative (**13a**), naphthalene derivative (**13q**), thiophene derivative (**13r**), pyridine derivatives (**13s** and **13t**), and indole derivative (**13u**) showed lower potencies as compared to diminished activities, which indicated the importance of the A-ring scaffold. Among them, benzene derivative (**13a**) exhibited the highest cytotoxicity with an average IC_{50} value of 11.6 μM against the three cancer cells. Subsequently, we concentrated on systematic modification of phenyl to explore the variations in position and type of substituents. Replacement of hydrogen atom in **13a** with methyl (**13b**, **13c**, and **13d**), methoxyl (**13f**, **13g**, and **13h**), ethyoxyl (**13l**), or hydroxyl (**13p**) resulted in compounds with similar or stronger potencies than **13a**. Compound **13h** exhibited the highest antiproliferative activity with mean IC_{50} value ranging from 3.4 μM to 5.5 μM, at least 3-fold more potent than **13a**, indicating that 4-position methoxyl in phenyl A-ring is optimal for activity. Next, the introduction of electron-withdrawing groups, such as fluorine (**13m**), chlorine (**13n**), or nitro (**13o**) in the 4-position methoxy portion of compound **13h** reduced the inhibitory activities to varying degrees. In addition, the triple substituted compound showed increased activity, which could be confirmed by compound **13k**. Among the target compounds, compound **13k** (A-ring = 3,4,5-trimethoxyphenyl) showed the best antiproliferative activity against HeLa cells with an IC_{50} value of 1.2 ± 0.09 μM.

2.2.2. *Effect on tubulin polymerization*

To investigate the relationship between the antiproliferative activities of these compounds and tubulin, we evaluated the effect of the most active compound **13k** on tubulin polymerization compared to the positive control CA-4 and the negative control paclitaxel. As shown in Fig. 3, both CA-4 and **13k** exhibited significant inhibition of tubulin polymerization. In comparison, paclitaxel enhanced the rate of tubulin polymerization. These results demonstrated that **13k** interferes with tubulin polymerization.

2.2.3. *Analysis of immunofluorescence staining*

To examine whether compound **13k** can interfere with microtubule dynamics, an immunofluorescence assay was performed in HeLa cells treated with **13k**. As presented in Fig. 4, the control cells exhibited normal organization and arrangement with

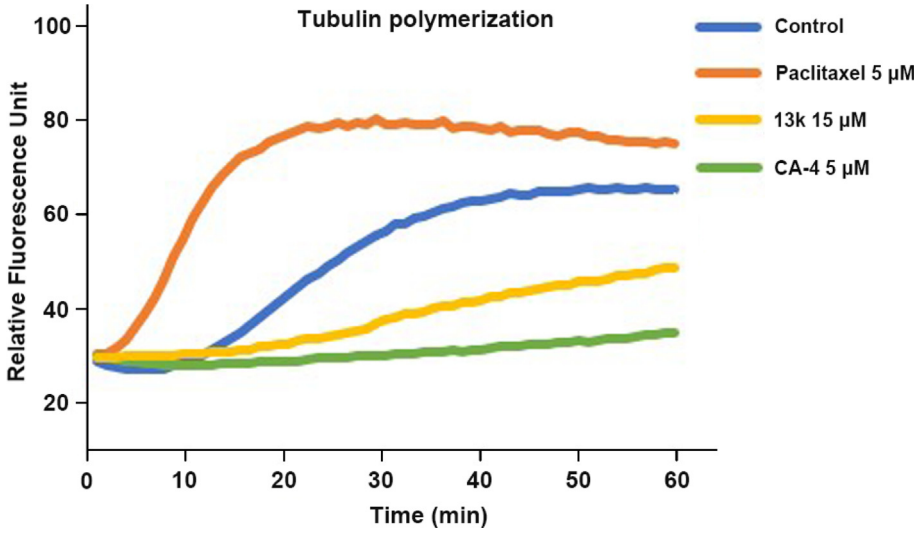

Fig. 3 Effects of compound **13k** on tubulin polymerization.

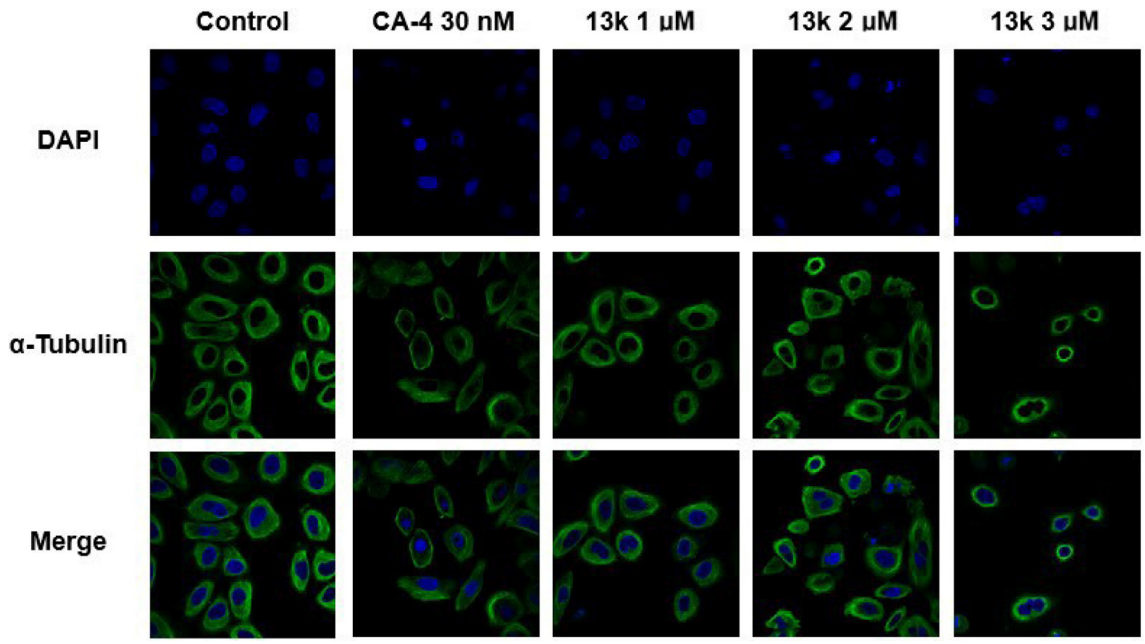

Fig. 4 Effects of compound **13k** (1 μM, 2 μM, and 3 μM) and CA-4 (30 nM), on the cellular microtubule network and microtubule reassemble by immunofluorescence.

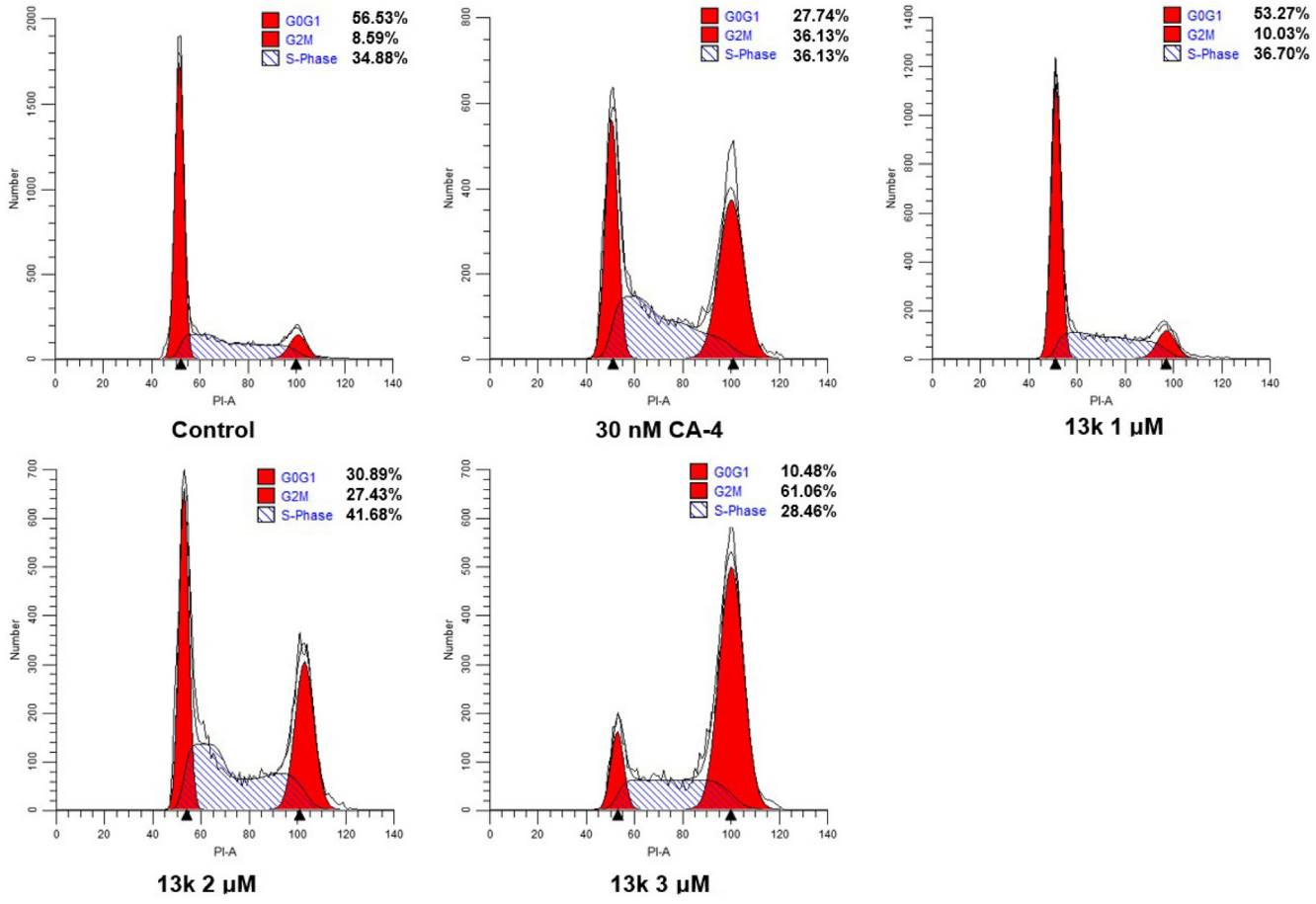

Fig. 5 Effects of CA-4 and compound **13k** on cell cycle. HeLa cell lines were treated with CA-4 (30 nM) and compound **13k** (1 μM, 2 μM, and 3 μM) for 24 h.

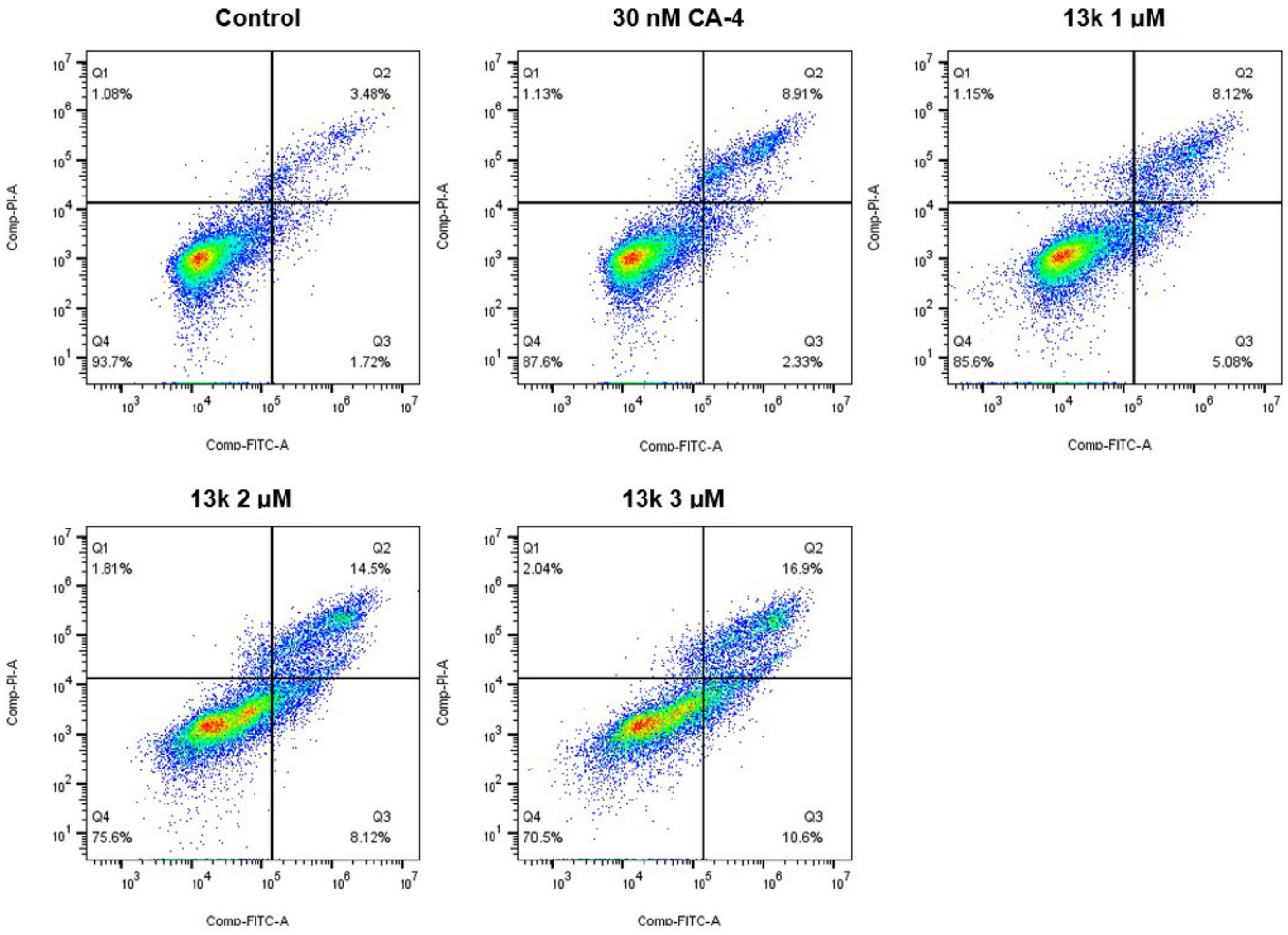

Fig. 6 Analyses of apoptosis induction in Hela cells. Cells were harvested and stained with Annexin-V/PI for analysis after treatment with different concentrations of compound **13k** (1, 2, and 3 μM) and control for 48 h. The diverse cell stages were given as live (Q4), early apoptotic (Q3), late apoptotic (Q2), and necrotic cells (Q1).

hairy, elongated, and fibrous microtubules (green) wrapped around the nucleus (blue). However, after treatment with CA-4 (30 nM) or **13k** (1 μM, 2 μM, and 3 μM) for 24 h, the microtubules became short and disintegrated, indicating that the microtubule network was disrupted. These results implied that **13k** could destabilize microtubules by inducing the depolymerization and collapse of the microtubule network, similar to CA-4.

2.2.4. Cell cycle analysis

Tubulin polymerization inhibitors are known to induce cell cycle arrest in the G2/M phase (Shi et al., 2022). To explore the effect of compound **13k** on the cell cycle, flow cytometric analysis was performed on HeLa cells treated with **13k**. As demonstrated in Fig. 5, the percentage of cells stalled in G2/M phase increased from 10.03% to 61.06% after treatment with different concentrations of **13k** (1 μM, 2 μM, and 3 μM) for 24 h compared to the control (8.59%). Thus, **13k** could concentration-dependently induce G2/M phase arrest in HeLa cells.

2.2.5. Induction of cell apoptosis

It has been shown that tubulin polymerization inhibitors can induce apoptosis (Wang et al., 2019; Yang et al., 2022). Therefore, we investigated the effect of compound **13k** on apoptosis in HeLa cells. As illustrated in Fig. 6, when HeLa cells were treated with different concentrations (1 μM, 2 μM, and 3 μM) of **13k** for 48 h, the percentage of total apoptotic cells increased significantly and concentration-dependently, from 5.20% (control) to 13.20% (1 μM), 22.62% (2 μM), and 27.50% (3 μM), respectively.

2.2.6. Molecular docking analysis

To understand the possible binding modes of the target compounds, a molecular docking analysis of compound **13k** was conducted by using the CDOCKER program of Discovery Studio 3.0 software (PDB: 1SA0). The docking study indicated that **13k** occupied the colchicine binding sites of α- and β-tubulin and was mainly buried in the β-subunit (Fig. 7). For **13k**, a hydrogen bond was formed between the oxygen atom of methoxy and the residue of ALAβ250. In addition, the nitrogen atom of carbazole formed another hydrogen bond

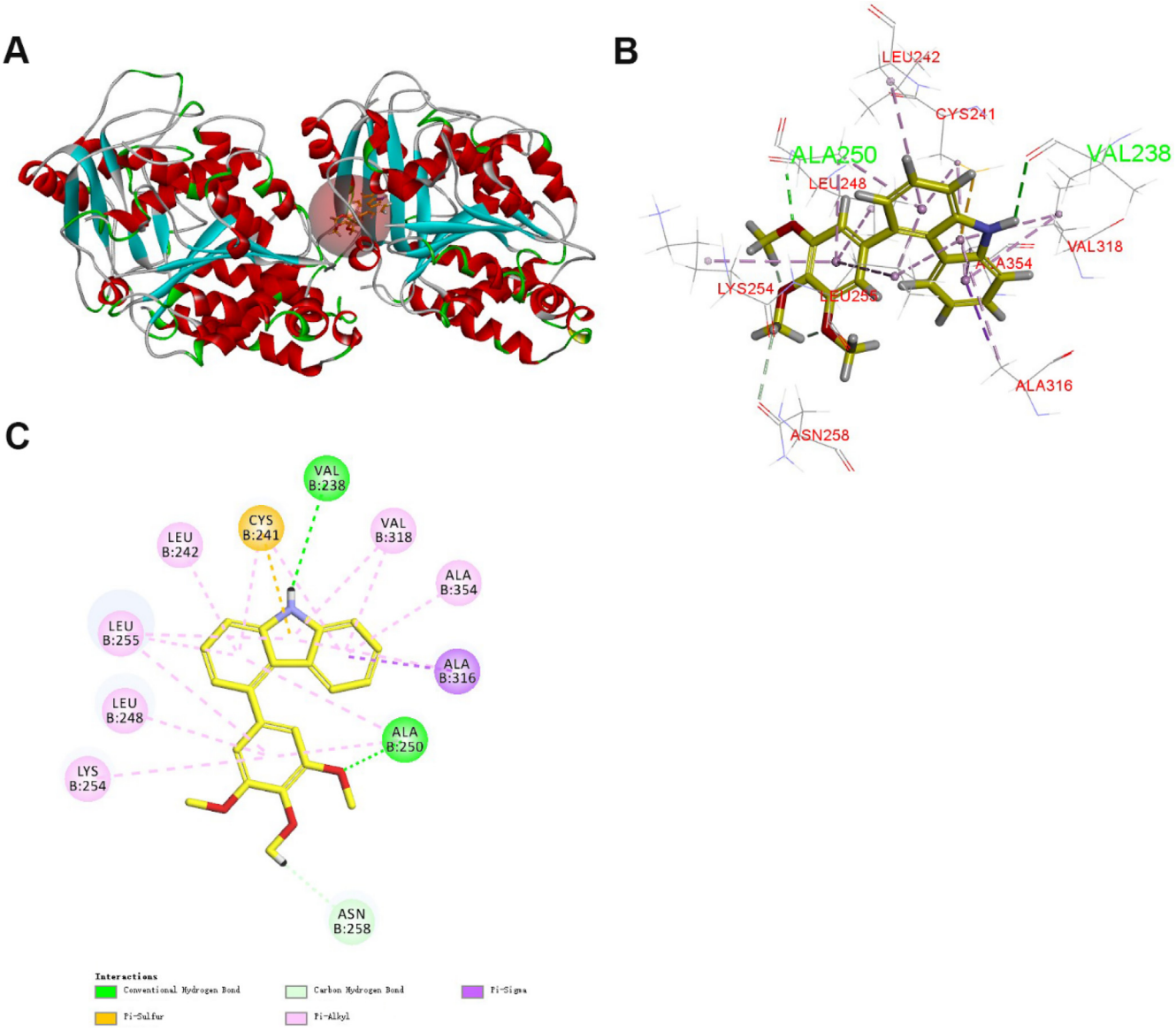

Fig. 7 (A) Predicted mode for compound **13k** (yellow) binding in the colchicine binding site of tubulin (PDB: 1SA0); (B and C) Docking conformation of compound **13k** in the colchicine binding site of tubulin.

Table 2 Prediction of physicochemical properties[a] of **9** and **13k.**

Compounds	cLogP	TPSA	natoms	MW	HBA	HBD
Standard	< 5	< 140		< 500	< 10	< 5
9	4.43	29.54	31	281.32	3	1
13 k	4.70	39.72	44	333.39	3	1

[a] cLogP: calculated logarithm of the octanol–water partition coefficient; TPSA: topological polar surface area; natoms: No. of atoms; MW: molecular weight; HBA: hydrogen-bond acceptor atoms. HBD: hydrogen-bond donor atoms.

with the residue of VALβ238. These results point to a possible binding of **13k** to the colchicine binding site on tubulin.

2.2.7. Physicochemical properties

To explore the drug-like properties of the target compounds, some physicochemical properties of **9** and **13k** were predicted using the ChemBioDraw Ultra 14.0 software or free online website (https://www.swissadme.ch/index.php) for their adaptability with Lipinski's rule of five. As shown in Table 2, 9 and 13**k** conform well to the Lipinski's rule of five. Additionally, **13k** exists three hydrogen bond acceptors and one hydrogen

bond donor, which helps to reduce the binding energy between the compound and the action site.

3. Conclusion

In conclusion, we developed a family of new carbazole-containing tubulin polymerization inhibitors. These compounds exhibited moderate to high antiproliferative potencies against a diverse set of cancer cell lines (HeLa, HepG2, and SGC-7901 cells). With IC_{50} values in the micromole range (1.2–2.2 μM), compound **13k** demonstrated the strongest activities against the three cancer cell lines. Additionally, **13k** was able to inhibit tubulin polymerization *in vitro*. Preliminary mechanistic studies revealed that **13k** induced G2/M phase cell cycle arrest and apoptosis in HeLa cells. Further mechanistic studies illustrated that **13k** could effectively disrupt the microtubule networks in HeLa cells in a concentration-dependent manner. Molecular docking analysis indicated that **13k** bound well to the colchicine binding site, which might explain the high antiproliferative activity of **13k**. Finally, the prediction of physicochemical properties studies shows that **13k** has good pharmacokinetic properties. In summary, these results suggest that **13k** is a promising tubulin polymerization inhibitor that deserves further investigation.

4. Experimental

4.1. Chemistry

4.1.1. Materials and methods

All of the reagents and solvents were purchased from chemical companies. ^{1}H NMR and ^{13}C NMR spectra were tested in $CDCl_3$ with TMS as the internal reference on a Bruker AVANCE (^{1}H at 500 MHz, ^{13}C at 126 MHz). Mass spectra (MS) were measured on an Agilent 1100-sl mass spectrometer with an electrospray ionization source from Agilent Co. Ltd.. TLC analysis was used for determining the extent of reactions under UV light (wavelength: 365 nm and 254 nm).

4.1.2. General synthetic procedure for 2-bromo-2′-nitro-1,1′-biphenyl (*16*)

To a stirring solution of 1-bromo-2-nitrobenzene (**14**, 4.95 mmol) and (2-bromophenyl)boronic acid (**15**, 5.45 mmol) in THF (15 ml) were added $Pd(PPh_3)_4$ (0.25 mmol) followed by K_2CO_3 (0.05 mmol in 10 ml water) at room temperature. The reaction mixture was degassed and purged with N_2 about three times and was stirred at irradiated in a microwave reactor for 20 min at 116 °C after which it was cooled and extracted with dichloromethane. The combined organic layer was dried over Na_2SO_4, filtered, and concentrated in vacuo. The crude material was purified by column chromatography over silica gel using *n*-hexane/ethyl acetate (9:1) as a solvent to give 2-brom o-2′-nitro-1,1′-biphenyl (**16**).

4.1.3. General synthetic procedure for4-bromo-9H-carbazole (*17*)

2-bromo-2′-nitro-1,1′-biphenyl (**16**, 1.01 mmol) and triphenylphosphine (2.6 mmol) were dissolved in 1,2-dichlorobenzene (10 ml), and the resulting solution was stirred at 170 °C for 12 h, after which it was cooled and extracted with dichloromethane/H_2O. The combined organic layer was dried over Na_2SO_4, filtered, and concentrated in vacuo. The crude material was purified by column chromatography over silica gel using *n*-hexane/ethyl acetate (8:1) to yield 4-bromo-9*H*-carbazole (**17**).

4.1.4. General synthetic procedure for 4-aryl-9H-carbazoles (*13a-u*)

A mixture of 4-bromo-9*H*-carbazole (**17**, 0.10 mmol), Pd $(PPh_3)_4$ (0.005 mmol), and K_2CO_3 (0.12 mmol), and substituted phenylboronic acid (0.11 mmol) in 1,4-dioxane/H_2O (5 ml, 3:1) was degassed and purged with N_2 for about three times. After stirring at irradiated in a microwave reactor for 25 min at 130 °C (indicated by TLC) under N_2 atmosphere, H_2O (50 ml) was added to the reaction mixture and extracted with ethyl acetate. The combined organics were washed with brine, dried over anhydrous Na_2SO_4, filtered, and concentrated under vacuum to give a residue, which was purified by column 400 chromatography using a mixture of *n*-hexane/ethyl acetate (3:1) as an eluent to provide the target compounds 4-aryl-9*H*-carbazoles (**13a-v**).

*4.1.4.1. 4-phenyl-9H-carbazole (**13a**).* White solid; yield: 63.1%; ^{1}H NMR (500 MHz, $CDCl_3$) δ 8.13 (s, 1H), 7.69–7.63 (m, 2H), 7.57–7.52 (m, 2H), 7.52–7.47 (m, 2H), 7.47–7.45 (m, 1H), 7.44–7.40 (m, 2H), 7.37 (ddd, J = 8.1, 7.1, 1.1 Hz, 1H), 7.13 (dd, J = 7.1, 1.1 Hz, 1H), 7.00 (ddd, J = 8.1, 7.1, 1.1 Hz, 1H); ^{13}C NMR (126 MHz, $CDCl_3$) δ 141.3, 139.8, 139.7, 137.8, 129.2 (2C), 128.4 (2C), 127.5, 125.7 (2C), 122.9, 122.4, 121.1, 120.8, 119.0, 110.4, 109.5; MS (ESI) m/z 244.0 $[M + H]^+$.

*4.1.4.2. 4-(o-tolyl)-9H-carbazole (**13b**).* Light yellow solid; yield: 95.0%; ^{1}H NMR (500 MHz, $CDCl_3$) δ 8.08 (s, 1H), 7.52–7.46 (m, 1H), 7.42 (ddd, J = 15.3, 8.7, 5.1 Hz, 4H), 7.38–7.33 (m, 3H), 7.07 (d, J = 7.2 Hz, 1H), 7.00–6.95 (m, 2H), 2.12 (s, 3H); ^{13}C NMR (126 MHz, $CDCl_3$) δ 140.8, 139.5, 139.4, 136.9, 136.4, 130.0, 129.5, 127.7, 125.9, 125.6 (2C), 123.2, 121.8, 121.4, 120.5, 119.4, 110.3, 109.3, 19.8; MS (ESI) m/z 258.1 $[M + H]^+$.

*4.1.4.3. 4-(m-tolyl)-9H-carbazole (**13c**).* White solid; yield: 95.2%; ^{1}H NMR (500 MHz, $CDCl_3$) δ 8.10 (s, 1H), 7.53 (d, J = 8.0 Hz, 1H), 7.46 (ddd, J = 9.9, 4.7, 2.9 Hz, 4H), 7.42 (dd, J = 6.3, 5.4 Hz, 2H), 7.39–7.35 (m, 1H), 7.32 (d, J = 7.0 Hz, 1H), 7.14 (dd, J = 7.2, 1.0 Hz, 1H), 7.02 (ddd, J = 8.1, 6.9, 1.2 Hz, 1H), 2.48 (s, 3H); ^{13}C NMR (126 MHz, $CDCl_3$) δ 141.2, 139.8, 139.7, 138.0, 137.9, 129.9, 128.3, 128.2, 126.2, 125.6 (2C), 123.0, 122.5, 121.0, 120.8, 119.1, 110.4, 109.4, 21.5; MS (ESI) m/z 258.1 $[M + H]^+$, 282.2 $[M + Na]^+$.

*4.1.4.4. 4-(p-tolyl)-9H-carbazole (**13d**).* White solid; yield: 95.7%; ^{1}H NMR (500 MHz, $CDCl_3$) δ 8.11 (s, 1H), 7.59–7.54 (m, 3H), 7.49–7.44 (m, 1H), 7.42–7.39 (m, 2H), 7.37 (dd, J = 11.7, 4.6 Hz, 3H), 7.13 (dd, J = 7.2, 1.0 Hz, 1H), 7.02 (ddd, J = 8.1, 7.0, 1.3 Hz, 1H), 2.52 (s, 3H); ^{13}C NMR (126 MHz, $CDCl_3$) δ 139.8, 139.7, 138.3, 137.8, 137.1, 129.1 (4C), 125.6 (2C), 123.0, 122.5, 121.2, 120.8, 119.0, 110.4, 109.3, 21.4; MS (ESI) m/z 258.0 $[M + H]^+$, 282.1 $[M + Na]^+$.

*4.1.4.5. 4-(3,4-dimethylphenyl)-9H-carbazole (**13e**).* Light yellow solid; yield: 97.1%; ^{1}H NMR (500 MHz, $CDCl_3$) δ 8.08 (s, 1H), 7.60 (d, J = 8.0 Hz, 1H), 7.49–7.43 (m, 2H), 7.44–7.35

(m, 4H), 7.32 (d, J = 7.6 Hz, 1H), 7.13 (dd, J = 7.3, 0.9 Hz, 1H), 7.03 (ddd, J = 8.1, 6.7, 1.4 Hz, 1H), 2.43 (s, 3H), 2.39 (s, 3H); ^{13}C NMR (126 MHz, $CDCl_3$) δ 139.9, 139.7, 138.8, 137.9, 136.5, 135.8, 130.4, 129.6, 126.6, 125.6, 125.5, 123.1, 122.6, 121.1, 120.8, 119.0, 110.3, 109.3, 19.8, 19.7; MS (ESI) m/z 272.1 $[M + H]^+$.

*4.1.4.6. 4-(2-methoxyphenyl)-9H-carbazole (**13f**)*. White solid; yield: 94.0%; ^{1}H NMR (500 MHz, $CDCl_3$) δ 8.05 (s, 1H), 7.47 (ddd, J = 13.1, 5.2, 4.0 Hz, 2H), 7.41 (dd, J = 7.4, 1.7 Hz, 1H), 7.38–7.30 (m, 3H), 7.20 (d, J = 8.0 Hz, 1H), 7.12 (dd, J = 16.3, 7.9 Hz, 3H), 6.97 (ddd, J = 8.1, 6.4, 1.8 Hz, 1H), 3.67 (s, 3H); ^{13}C NMR (126 MHz, $CDCl_3$) δ 157.1, 139.6, 139.5, 136.8, 133.7, 132.9, 131.2, 130.1, 129.1, 125.4 (2C), 122.1, 121.3, 120.7, 119.0, 110.9, 110.2, 109.5, 55.6; MS (ESI) m/z 274.1 $[M + H]^+$, 296.0 $[M + Na]^+$.

*4.1.4.7. 4-(3-methoxyphenyl)-9H-carbazole (**13g**)*. Light yellow solid; yield: 87.4%; ^{1}H NMR (500 MHz, $CDCl_3$) δ 8.14 (s, 1H), 7.57 (d, J = 8.0 Hz, 1H), 7.46 (td, J = 8.0, 2.2 Hz, 2H), 7.43—7.34 (m, 3H), 7.25 (d, J = 8.0 Hz, 1H), 7.20 (s, 1H), 7.15 (d, J = 7.1 Hz, 1H), 7.08–7.00 (m, 2H), 3.87 (s, 3H); ^{13}C NMR (126 MHz, $CDCl_3$) δ 159.6, 142.7, 139.8, 139.7, 137.6, 129.4, 125.7, 125.6, 122.9, 122.6, 121.7, 120.9, 120.7, 119.1, 114.3, 113.5, 110.4, 109.6, 55.3; MS (ESI) m/z 274.1 $[M + H]^+$, 296.1 $[M + Na]^+$.

*4.1.4.8. 4-(4-methoxyphenyl)-9H-carbazole (**13 h**)*. White solid; yield: 90.0%; ^{1}H NMR (500 MHz, $CDCl_3$) δ 8.12 (s, 1H), 7.62–7.54 (m, 3H), 7.45 (dd, J = 8.0, 7.3 Hz, 1H), 7.42–7.34 (m, 3H), 7.14–7.06 (m, 3H), 7.02 (ddd, J = 8.1, 6.8, 1.4 Hz, 1H), 3.95 (s, 3H); ^{13}C NMR (126 MHz, $CDCl_3$) δ 159.1, 139.9, 139.7, 137.5, 133.7, 130.3 (2C), 125.6 (2C), 123.1, 122.4, 121.2, 120.9, 119.0, 113.8 (2C), 110.4, 109.2, 55.4; MS (ESI) m/z 274.1 $[M + H]^+$.

*4.1.4.9. 5-(9H-carbazol-4-yl)-2-methoxyphenol (**13i**)*. White solid; yield: 96.1%; ^{1}H NMR (500 MHz, $CDCl_3$) δ 8.13 (s, 1H), 7.63 (d, J = 8.0 Hz, 1H), 7.40 (qd, J = 15.3, 7.8 Hz, 4H), 7.24 (d, J = 1.8 Hz, 1H), 7.16–7.07 (m, 2H), 7.02 (t, J = 8.3 Hz, 2H), 5.75 (s, 1H), 4.01 (s, 3H); ^{13}C NMR (126 MHz, $CDCl_3$) δ 146.1, 145.5, 139.8, 139.7, 137.4, 134.7, 125.6, 125.5, 123.0, 122.6, 121.1, 120.9, 120.8, 119.0, 115.6, 110.5, 110.3, 109.3, 56.1; MS (ESI) m/z 290.1 $[M + H]^+$, 312.9 $[M + Na]^+$.

*4.1.4.10. 4-(3,4-dimethoxyphenyl)-9H-carbazole (**13j**)*. White solid; yield: 89.6%; ^{1}H NMR (500 MHz, $CDCl_3$) δ 8.20 (s, 1H), 7.58 (d, J = 8.0 Hz, 1H), 7.50–7.39 (m, 3H), 7.39–7.32 (m, 1H), 7.19 (td, J = 4.3, 1.9 Hz, 2H), 7.13 (dd, J = 6.9, 1.3 Hz, 1H), 7.07–7.03 (m, 1H), 7.03–6.98 (m, 1H), 4.01 (s, 3H), 3.88 (s, 3H); ^{13}C NMR (126 MHz, $CDCl_3$) δ 148.6, 148.5, 139.9, 139.7, 137.5, 134.0, 125.6 (2C), 123.0, 122.5, 121.2, 121.0, 120.9, 119.0, 112.6, 111.2, 110.4, 109.4, 56.0, 55.9; MS (ESI) m/z 304.1 $[M + H]^+$, 326.1 $[M + Na]^+$.

*4.1.4.11. 4-(3,4,5-trimethoxyphenyl)-9H-carbazole (**13k**)*. White solid; yield: 82.6%; ^{1}H NMR (500 MHz, $CDCl_3$) δ 8.31 (s, 1H), 7.63 (d, J = 8.0 Hz, 1H), 7.48–7.40 (m, 3H), 7.38 (t, J = 7.6 Hz, 1H), 7.15 (dd, J = 6.8, 1.3 Hz, 1H), 7.04 (t, J = 7.5 Hz, 1H), 6.88 (s, 2H), 4.01 (s, 3H), 3.87 (s, 6H); ^{13}C NMR (126 MHz, $CDCl_3$) δ 153.1 (2C), 139.9, 139.8, 137.6, 137.4, 136.9, 125.7, 125.5, 122.8, 122.6, 120.7 (2C), 119.1, 110.5, 109.7, 106.2 (2C), 61.1, 56.2 (2C); MS (ESI) m/z 334.1 $[M + H]^+$, 356.1 $[M + Na]^+$.

*4.1.4.12. 4-(4-ethoxyphenyl)-9H-carbazole (**13l**)*. White solid; yield: 51.2%; ^{1}H NMR (500 MHz, $CDCl_3$) δ 8.14 (s, 1H), 7.60–7.53 (m, 3H), 7.47–7.38 (m, 3H), 7.38–7.32 (m, 1H), 7.10 (dd, J = 7.1, 1.1 Hz, 1H), 7.09–7.04 (m, 2H), 7.04–6.97 (m, 1H), 4.17 (q, J = 7.0 Hz, 2H), 1.51 (t, J = 7.0 Hz, 3H); ^{13}C NMR (126 MHz, $CDCl_3$) δ 158.5, 139.8, 139.7, 137.5, 133.5, 130.3 (2C), 125.6, 125.5, 123.1, 122.5, 121.2, 120.9, 119.0, 114.3 (2C), 110.3, 109.2, 63.5, 15.0; MS (ESI) m/z 288.1 $[M + H]^+$.

*4.1.4.13. 4-(4-fluorophenyl)-9H-carbazole (**13m**)*. White solid; yield: 85.3%; ^{1}H NMR (500 MHz, $CDCl_3$) δ 8.13 (s, 1H), 7.64–7.58 (m, 2H), 7.45 (ddd, J = 16.5, 9.2, 5.1 Hz, 4H), 7.40–7.35 (m, 1H), 7.23 (ddd, J = 9.5, 5.8, 2.5 Hz, 2H), 7.10 (dd, J = 7.0, 1.2 Hz, 1H), 7.03 (ddd, J = 8.1, 6.9, 1.2 Hz, 1H); ^{13}C NMR (126 MHz, $CDCl_3$) δ 162.5, 139.8, 139.7, 137.2 (2C), 136.6, 130.8 (2C), 125.8, 125.6, 122.8, 122.2, 121.1, 119.1, 115.3 (2C), 110.5, 109.7; MS (ESI) m/z 262.0 $[M + H]^+$, 284.2 $[M + Na]^+$.

*4.1.4.14. 4-(4-chlorophenyl)-9H-carbazole (**13n**)*. Light yellow solid; yield: 97.3%; ^{1}H NMR (500 MHz, $CDCl_3$) δ 8.14 (s, 1H), 7.60–7.56 (m, 2H), 7.54–7.47 (m, 3H), 7.43 (ddd, J = 8.1, 7.6, 4.8 Hz, 3H), 7.41–7.36 (m, 1H), 7.09 (dd, J = 6.9, 1.3 Hz, 1H), 7.04 (ddd, J = 8.1, 7.1, 1.3 Hz, 1H); ^{13}C NMR (126 MHz, $CDCl_3$) δ 139.8, 139.7 (2C), 136.4, 133.5, 130.6 (2C), 129.8, 129.0, 128.6 (2C), 125.8, 125.7, 122.3, 121.1, 119.2, 110.5, 109.9; MS (ESI) m/z 279.0 $[M + H]^+$, 301.0 $[M + Na]^+$.

*4.1.4.15. 4-(4-nitrophenyl)-9H-carbazole (**13o**)*. Yellow Solid; yield: 85.5%; ^{1}H NMR (500 MHz, $CDCl_3$) δ 8.46–8.35 (m, 2H), 8.27 (s, 1H), 7.86–7.79 (m, 2H), 7.50 (ddd, J = 22.8, 12.0, 4.7 Hz, 3H), 7.40 (dt, J = 8.1, 4.5 Hz, 2H), 7.10 (dd, J = 6.8, 1.4 Hz, 1H), 7.05–6.99 (m, 1H); ^{13}C NMR (126 MHz, $CDCl_3$) δ 148.2, 147.4, 139.4, 139.8, 135.1, 130.2 (2C), 126.2, 125.7, 123.7 (2C), 122.2, 122.0, 121.0, 120.2, 119.4, 110.8 (2C); MS (ESI) m/z 288.1 $[M + H]^+$.

*4.1.4.16. 4-(9H-carbazol-4-yl)phenol (**13p**)*. White solid; yield: 82.4%; ^{1}H NMR (500 MHz, $CDCl_3$) δ 8.13 (s, 1H), 7.57 (d, J = 8.0 Hz, 1H), 7.55–7.49 (m, 2H), 7.49–7.33 (m, 4H), 7.10 (dd, J = 7.2, 0.8 Hz, 1H), 7.06–6.97 (m, 3H), 5.05 (s, 1H); ^{13}C NMR (126 MHz, $CDCl_3$) δ 155.0, 139.9, 139.7, 137.4, 133.9, 130.5 (2C), 125.6 (2C), 123.0, 122.4, 121.1, 120.9, 119.0, 115.3 (2C), 110.4, 109.3; MS (ESI) m/z 260.0 $[M + H]^+$, 282.2 $[M + Na]^+$.

*4.1.4.17. 4-(naphthalen-2-yl)-9H-carbazole (**13q**)*. Light yellow solid; yield: 90.7%; ^{1}H NMR (500 MHz, $CDCl_3$) δ 8.14 (d, J = 5.9 Hz, 2H), 8.06–7.97 (m, 2H), 7.97–7.91 (m, 1H), 7.82 (dd, J = 8.4, 1.7 Hz, 1H), 7.62–7.54 (m, 2H), 7.54–7.48 (m, 2H), 7.44 (dd, J = 16.7, 7.7 Hz, 2H), 7.40–7.33 (m, 1H), 7.27–7.21 (m, 1H), 6.99–6.92 (m, 1H); ^{13}C NMR (126 MHz, $CDCl_3$) δ 139.9, 139.7, 138.8, 137.6, 133.6, 132.8, 128.2, 127.9, 127.8 (2C), 127.7, 126.2, 126.0, 125.7 (2C), 122.9, 122.5, 121.4, 120.9, 119.1, 110.4, 109.7; MS (ESI) m/z 294.0 $[M + H]^+$, 316.1 $[M + Na]^+$.

*4.1.4.18. 4-(thiophen-3-yl)-9H-carbazole (**13r**).* Light yellow solid; yield: 92.2%; ^{1}H NMR (500 MHz, $CDCl_3$) δ 8.11 (s, 1H), 7.66 (d, J = 8.0 Hz, 1H), 7.51 (ddd, J = 4.3, 3.9, 2.2 Hz, 2H), 7.47–7.36 (m, 5H), 7.18 (dd, J = 7.0, 1.2 Hz, 1H), 7.07 (ddd, J = 8.1, 6.6, 1.6 Hz, 1H); ^{13}C NMR (126 MHz, $CDCl_3$) δ 141.7, 139.8, 139.6, 132.4, 129.1, 125.7, 125.5, 125.4, 123.0, 122.8, 122.4, 121.2 (2C), 119.2, 110.4, 109.7; MS (ESI) m/z 250.0 $[M + H]^+$.

*4.1.4.19. 4-(pyridin-3-yl)-9H-carbazole (**13s**).* Light yellow solid; yield: 87.4%; ^{1}H NMR (500 MHz, $CDCl_3$) δ 8.94 (s, 1H), 8.78 (s, 1H), 8.65 (s, 1H), 7.99 (d, J = 7.8 Hz, 1H), 7.55–7.47 (m, 3H), 7.46–7.41 (m, 2H), 7.40–7.34 (m, 1H), 7.13–7.06 (m, 1H), 7.01 (t, J = 7.5 Hz, 1H); ^{13}C NMR (126 MHz, $CDCl_3$) δ 149.7, 148.5, 140.0, 139.8, 137.2, 136.9, 133.5, 126.0, 125.7, 123.4, 122.5, 122.0, 121.3, 120.8, 119.3, 110.7, 110.5; MS (ESI) m/z 245.0 $[M + H]^+$.

*4.1.4.20. 4-(pyridin-4-yl)-9H-carbazole (**13 t**).* White solid; yield: 33.9%; ^{1}H NMR (500 MHz, $CDCl_3$) δ 8.84 (s, 2H), 8.36 (s, 1H), 7.65 (s, 2H), 7.54–7.44 (m, 4H), 7.42–7.37 (m, 1H), 7.10 (dd, J = 6.9, 1.2 Hz, 1H), 7.06–7.00 (m, 1H); ^{13}C NMR (126 MHz, $CDCl_3$) δ 149.7, 149.4, 140.4, 139.9, 139.8, 134.4, 126.2, 125.7, 124.7, 124.5, 122.1 (2C), 120.8, 120.0, 119.4, 110.9, 110.7; MS (ESI) m/z 245.0 $[M + H]^+$.

*4.1.4.21. 4-(1H-indol-4-yl)-9H-carbazole (**13u**).* White solid; yield: 56.7%; ^{1}H NMR (500 MHz, $CDCl_3$) δ 8.26 (s, 1H), 8.16 (s, 1H), 7.54–7.45 (m, 3H), 7.42–7.32 (m, 3H), 7.29 (td, J = 7.0, 1.3 Hz, 2H), 7.20–7.13 (m, 1H), 7.08 (d, J = 8.0 Hz, 1H), 6.89–6.79 (m, 1H), 6.27 (t, J = 2.2 Hz, 1H); ^{13}C NMR (126 MHz, $CDCl_3$) δ 139.9, 139.7, 136.3, 135.9, 133.6, 127.2, 125.5, 125.4, 124.2, 123.1, 123.0, 122.1, 121.5, 121.4, 120.6, 118.9, 110.3, 110.0, 109.3, 102.9; MS (ESI) m/z 283.0 $[M + H]^+$.

4.2. Biological evaluation

4.2.1. Cell culture

HeLa, HepG2, and SGC-7901 cells were cultured in RPMI-1640 medium containing 10% FBS, 100 U/mL streptomycin, and 100 U/mL penicillin at 37 °C in a humidified atmosphere containing 5% CO_2. All cell lines were purchased from the American Type Culture Collection (ATCC, Manassas, VA).

4.2.2. In vitro antiproliferative activity

The *in vitro* antiproliferative activities of CA-4 and all of the target compounds were determined by MTT assay (Tan et al., 2023). Briefly, cells were seeded into 96-well plates at a density of 2 × 10^4/well, depending on the growth rate of the cell line. 24 h later, triplicate wells were treated with media and the compounds being tested. After 72 h of incubation at 37℃ in 5% CO_2, the drug-containing medium was removed and replaced with 100 μL of fresh medium containing 5 mg/mL MTT solution. After 4 h of incubation, the medium with MTT was removed, and 100 μL of dimethyl sulfoxide was added to each well. The plates were gently agitated until the purple formazan crystals were dissolved, and the OD_{490} values were determined using a microplate reader. The data were calculated and plotted as the percent viability compared to the control. The IC_{50} was defined as the drug concentration that resulted in an absorbance of 50% of that of the untreated wells in the MTT assay.

4.2.3. Effect on tubulin polymerization

The effects of compound **13k** and CA-4 on tubulin polymerization were determined using a fluorescence-based tubulin polymerisation assay kit (Cytoskeleton-Cat.#BK011P) according to the manufacturer's protocol (Chen et al., 2020). Tubulin was resuspended in ice-cold G-PEM buffer and added to wells of a 96-well plate containing the designated concentrations of the drug or vehicle. The samples were mixed well, and tubulin assembly was monitored at 1 min intervals for 90 min at 37℃ using a plate reader. The IC_{50} values were calculated after 20 min using SPSS software.

4.2.4. Analysis of immunofluorescence staining

Immunostaining was performed to detect the microtubule-associated tubulin protein after exposure to CA-4 and the investigated compound **13 k** (Deng et al., 2022). HeLa cells were seeded in a 24-well plate at 1 × 10^4 cells per well and grown for 24 h. The cells were treated with the vehicle, CA-4, or **13 k** for 24 h. The control and treated cells were fixed with 4% formaldehyde in PBS for 30 min at −20℃, washed twice with PBS and permeabilized with 0.1% (v/v) Triton X-100 in PBS for 5 min. The cells were then blocked with 5% bovine serum albumin in PBS for 10 min. The primary α-tubulin antibody was diluted (1/100) with 2% bovine serum albumin in PBS, and the plates were incubated overnight at 4℃. The cells were washed with PBS to remove unbound primary antibody, and the cells were then incubated with FITC-conjugated anti-mouse secondary antibody diluted (1/1000) with 2% BSA in PBS for 3 h at 37℃. The cells were washed with PBS to remove unbound secondary antibody, and the nuclei were stained with DAPI. Then, immunofluorescence was detected using a fluorescence microscope.

4.2.5. Cell cycle analysis

Cell cycle analysis studies were performed according to procedures described previously (Deng et al., 2022). Briefly, HeLa cells (8 × 10^4 cells) were incubated with various concentrations of CA-4, **13 k** or 0.05% DMSO for the indicated time. The cells were collected by centrifugation, washed with PBS and fixed in ice-cold 75% ethanol. The fixed cells were harvested by centrifugation and resuspended in 530 μL buffer containing 10 μL RNase (50 ×) and 25 μL PI (20 ×). After incubation at 37℃ in the dark for 30 min, the samples were then analyzed by FACScan flow cytometry (BectoneDickinson, Franklin Lakes, NJ, USA).

4.2.6. Induction of cell apoptosis

To investigate whether the target compound can induce apoptosis, an Annexin Van -FITC/PI experiment was carried out (Shi et al., 2022). HeLa cells were grown in 6-well plates (3 × 10^5 cells/well) and incubated with various concentrations of **13 k**, CA-4, or vehicle control for 48 h. Subsequently, cells were harvested by centrifugation, washed with PBS, and resuspended in binding buffer. Then, 10 μL of PI Staining Solution and 5 μL of Annexin V-FITC were added to the cell suspension for 15 min at room temperature in the dark. Finally, the samples were detected by a CytoFLEX flow cytometer

and the percentage of apoptotic cells was calculated using Flowjo 10.8 software.

4.3. Molecular docking analysis

The molecular modelling studies were performed with Accelrys Discovery Studio 3.0 (Yang et al., 2022). The crystal structure of tubulin complexed (PDB: 1SA0) was retrieved from the RCSB Protein Data Bank (https://www.rcsb.org/pdb). In the docking process, the protein protocol was prepared via several operations, including the standardization of atom names, insertion of missing atoms in residues and removal of alternate conformations, insertion of missing loop regions based on SEQRES data, optimization of short and medium sized loop regions with the Looper Algorithm, minimization of remaining loop regions, calculation of pK, and protonation of the structure. The receptor model was then typed with the CHARMm force field, and a binding sphere with a radius of 10 Å was defined with the original ligand as the binding site. **13 k** was drawn with Chemdraw and fully minimized using the CHARMm force field. Finally, they were docked into the binding site using the CDOCKER protocol with the default settings.

CRediT authorship contribution statement

Chao Wang, Yujing Zhang, and Dongming Xing downloaded the material and wrote original draft. **Shanbo Yang, Yutao Xiu, Wujun Chen, and Yanhong Wang** reviewed & edited the paper.

Declaration of Competing Interest

The authors declare that they have no known competing financial interests or personal relationships that could have appeared to influence the work reported in this paper.

Acknowledgements

This work was supported by grants from the Natural Science Foundation of Shandong (ZR2021QH156, China), the Medical and Health Science and Technology Development Plan Project of Shandong (202113051140, China), and the Key Project of Qingdao University Medical Group Scientific Research Project (YLJT20211014, China).

References

Ameen, S., Lee, S.B., Lee, Y.G., et al, 2018. 4-diphenylaminocarbazole: switching substituent position for voltage reduction and efficiency enhancement of OLEDs. ACS Appl. Mater. Interfaces. 10 (10), 8893–8900.

Arnst, K.E., Banerjee, S., Chen, H., et al, 2019. Current advances of tubulin inhibitors as dual acting small molecules for cancer therapy. Med. Res. Rev. 39, 1398–1426.

Banerjee, S., Arnst, K.E., Wang, Y., et al, 2018. Heterocyclic-fused pyrimidines as novel tubulin polymerization inhibitors targeting the colchicine binding site: structural basis and antitumor efficacy. J. Med. Chem. 61, 1704–1718.

Bzeih, T., Naret, T., Hachem, A., et al, 2016. A general synthesis of arylindoles and (1-arylvinyl)carbazoles via a one-pot reaction from N-tosylhydrazones and 2-nitro-haloarenes and their potential application to colon cancer. Chem. Commun. (Camb) 52 (88), 13027–13030.

Cermak, V., Dostal, V., Jelínek, M., et al, 2020. Microtubule-targeting agents and their impact on cancer treatment. Eur. J. Cell Biol. 99, 151075.

Chen, H., Deng, S.S., Wang, Y.X., et al, 2020. Structure-activity relationship study of novel 6-aryl-2-benzoylpyridines as tubulin polymerization inhibitors with potent antiproliferative properties. J. Med. Chem. 63, 827–846.

Deng, B., Sun, Z., Wang, Y., et al, 2022. Design, synthesis, and bioevaluation of imidazo [1,2-a] pyrazine derivatives as tubulin polymerization inhibitors with potent anticancer activities. Bioorg. Med. Chem. 76, 117098.

Dumontet, C., Jordan, M.A., 2010. Microtubule-binding agents: a dynamic field of cancer therapeutics. Nat. Rev. Drug Discov. 9, 790–803.

Egharevba, G.O., Kamal, A., Dosumu, O.O., et al, 2022. Synthesis and characterization of novel combretastatin analogues of 1,1-diaryl vinyl sulfones, with antiproliferative potential via in-silico and in-vitro studies. Sci. Rep. 12, 1901.

Elmabruk, A., Das, B., Yedlapudi, D., et al, 2019. Design, Synthesis, and pharmacological characterization of carbazole based dopamine agonists as potential symptomatic and neuroprotective therapeutic agents for parkinson's disease. ACS Chem. Neurosci. 10 (1), 396–411.

Hu, L., Li, Z.R., Wang, Y.M., et al, 2007. Novel pyridinyl and pyrimidinylcarbazole sulfonamides as antiproliferative agents. Bioorg. Med. Chem. Lett. 17 (5), 1193–1196.

Huang, L.C., Liu, M., Man, S., 2020. Design, synthesis and bioevaluation of novel 2-aryl-4-(3,4,5-trimethoxy-benzoyl)-5-substituted-1,2,3-triazoles as the tubulin polymerization inhibitors. Eur. J. Med. Chem. 186, 111846–111856.

Jordan, M., Wilson, A.L., 2004. Microtubules as a target for anticancer drugs. Nat. Rev. Cancer 4, 253–265.

Karahalil, B., Yardım-Akaydin, S., Nacak Baytas, S., 2019. An overview of microtubule targeting agents for cancer therapy. Arh. Hig. Rada. Toksikol. 70, 160–172.

Kaul, R., Risinger, A.L., Mooberry, S.L., 2019. Microtubule-targeting drugs: more than antimitotics. J. Nat. Prod. 82, 680–685.

Lawrence, E.J., Zanic, M., 2019. Rescuing microtubules from the brink of catastrophe: CLASPs lead the way. Curr. Opin. Cell Biol. 56, 94–101.

Lisowski, V., Léonce, S., Kraus-Berthier, L., et al, 2004. Design, synthesis, and evaluation of novel thienopyrrolizinones as antitubulin agents. J. Med. Chem. 47 (6), 1448–1464.

Lu, Y., Li, C.M., Ross, C.R., et al, 2009. Discovery of 4-substituted methoxybenzoylaryl-thiazole as novel anticancer agents: synthesis, biological evaluation, and structure-activity relationships. J. Med. Chem. 52, 1701–1711.

Naret, T., Khelifi, I., Provot, O., et al, 2019. 1,1-Diheterocyclic ethylenes derived from quinaldine and carbazole as new tubulin-polymerization inhibitors: synthesis, metabolism, and biological evaluation. J. Med. Chem. 62 (4), 1902–1916.

Risinger, A.L., 2011. ELR510444, a novel microtubule disruptor with multiple mechanisms of action. J. Pharmacol. Exp. Ter. 336, 652–660.

Sherbet, G.V., 2020. Combretastatin analogues in cancer biology: a prospective view. J. Cell. Biochem. 121, 2127–2138.

Shi, L., Yang, S., Chang, J., et al, 2022. Design, synthesis and biological evaluation of 9-aryl-5H-pyrido[4,3-b]indole derivatives as potential tubulin polymerization inhibitors. Front. Chem. 10, 1004835.

Steinmetz, M.O., Prota, A.E., 2018. Microtubule-targeting agents: strategies to hijack the cytoskeleton. Trends Cell Biol. 28, 776–792.

Tan, L., Wu, C., Zhang, J., et al, 2023. Design, synthesis, and biological evaluation of heterocyclic-fused pyrimidine chemotypes guided by X-ray crystal structure with potential antitumor and

anti-multidrug resistance efficacy targeting the colchicine binding site. J. Med. Chem. 66 (5), 3588–3620.
Wang, J., Miller, D.D., Li, W., 2022. Molecular interactions at the colchicine binding site in tubulin: an X-ray crystallography perspective. Drug Discov. Today 27 (3), 759–776.
Wang, C., Yang, S., Zhang, W.G., 2019. Synthesis and bioevaluation of diarylpyrazoles as antiproliferative agents. Eur. J. Med. Chem. 171, 1–10.
Wasylyk, C., Zheng, H., Castell, C., et al, 2008. Debussche, Inhibition of the Ras-Net (Elk-3) pathway by a novel pyrazole that affects microtubules. Cancer Res. 68, 1275–1283.
Yang, S., Wang, C., Shi, L., et al, 2022. Design, synthesis and biological evaluation of novel diarylpyridine derivatives as tubulin polymerisation inhibitors. J. Enzyme. Inhib. Med. Chem. 37 (1), 2755–2764.
Zhang, J., Tan, L., Wu, C., et al, 2023. Discovery and biological evaluation of 4,6-pyrimidine analogues with potential anticancer agents as novel colchicine binding site inhibitors. Eur. J. Med. Chem. 248, 115085.